Advances in Chemical Engineering and Science, **2011, 1, 1-8**
doi:10.4236/aces.2011.11001 Published Online January 2011 (http://www.SciRP.org/journal/aces)

Structural and Crystallographic Features of Chemically Synthesized Cero- and Titanium Cero- Antimonates Inorganic Ion Exchangers and Its Applications

Mamdouh M. Abou-Mesalam
Chemistry department, Faculty of Science, Al-Baha University, Kingdom Saudi Arabia
Nuclear Fuel Technology Department, Hot Labs. Centre, Atomic Energy Authority, Cairo, Egypt
E-mail: *mabumesalam@yahoo.com*
Received December 25, 2010; *revised January* 10, 2011; *accepted January* 15, 2011

Abstract

Chemically synthesized cero-antimonate and titanium cero-antimonate prepared by sol-gel technique was conducted for the synthesis of a novel ion exchanger. The prepared materials has been characterized by X-ray diffraction, X-ray fluorescence, Fourier transform Infrared Spectroscopy (FT-IR) and Thermogravemetric analyses. The structures and empirical formula's was identified and found to $CeSb_4O_{12}\cdot 6.19H_2O$ and $TiCeSb_4O_{14}\cdot 12.22H_2O$, for cero-antiomate and titanium cero-antimonate, respectively. The data obtained from X-ray diffraction was analyzed to define the crystallographic feature of cero-antimonate and titanium cero-antimonate and found both the composites were belong to cubic system with lattice constant 5.15 and 5.149 Å, respectively. The crystallite size and strain of cero-antimonate and titanium cero-antimonate were determined. By using ChemDraw Ultra program the modeling structures of cero-antimonate and titanium cero-antimonate were conducted. Finally, application of the prepared materials for the removal of heavy metals from industrial waste water in terms of capacity measurements was performed.

Keywords: Synthesis, Titanium Cero-Antimonate, Structure, Ion Exchanger, Composite

1. Introduction

The recent technologies in synthesis of ion exchange materials was attempted to find new materials with structure suitable for many purposes such as water purification and heavy metal removal from waste water effluents. Ion exchangers classified into organic and inorganic materials that were further differentiated into natural and synthetic exchangers [1-6]. In our previous publications a new category of a composite that contains organic and inorganic materials was synthesized such as magneso-silicate and magnesium alumino-silicate [7], lithium zirconium silicate [8], silico-antimonate [9], zirconium titanate [10], polyacrylamide acrylic acid - doped with silicon titanate [11], chromium and cerium titanates [12] and zirconium tin silicate [13]. The studies include complete characterization with some investigation for its applicability of inorganic and inorganic/organic materials for removing heavy metal and radionuclides from waste effluents.

The aim of conducting study is to prepare a new composite cero- and titanium cero-antimonates with complete characterization to investigate its structure and crystallographic features and its applicability to the removal of heavy metals from simulated industrial waste water. The crystallite size and grain due to doping of titanium with cero-antimonate was investigated. The empirical formulas, structures and the ion exchange capacities of the product materials conducted.

2. Experimental

2.1. Synthesis of Cero- Antimonate Ion Exchanger

Cero-antimonate was synthesized by the reaction of 1.0 M cerium ammonium nitrate (dissolved in distilled water) with 1.0 M antimony pentachloride with molar ratio Ce to Sb equal 1:1. The reaction carried out in water bath thermostat at 60°C with continuous stirring for 4 h. During the addition process, yellow gelatinous precipitate formed. After complete addition, few drops of diluted

ammonia solution were added for complete precipitation (pH~7) the precipitate left overnight standing for growth the fine particle. The precipitate separated by centrifugation at 3000 rpm and washed with 0.1 M HNO_3 to remove the excess Cl^- ions and impurities. Rewash the precipitate with distilled water to remove NO_3^- ions. Dry the precipitate in drying oven at 60°C. The granular solid poured in near boiling water (70-80°C) to remove the trapped air. The solids dried, grained, sieved and stored at room temperature.

2.2. Synthesis of Titanium Cero- Antimonate Ion Exchanger

Titanium tetrachloride solution with concentration 1.0 M was used for doped titanium in situ cero-antimonare. Titanium cero-antimonate solid sample was prepared by the reaction of 1.0 M titanium tetrachloride with a mixture of 1.0 M cerium ammonium nitrate and 1.0 M antimony pentachloride with volumetric ratio equal 1:1:1. The reaction carried out in water bath at 60°C with continuous stirring for 4h. Greenish yellow gelatinous precipitate formed during the addition process of titanium tetrachloride to the mixture. After an overnight standing the precipitate separated by centrifugation at 3000 rpm. The solids treated by 0.1 M HNO_3 to remove impurities and Cl^- ions. Solids rewashed with distilled water to remove NO_3^- ions. After drying in drying oven at 60°C, the granules solids poured in near boiling water at 70-80°C to remove the trapped air. Dry, grand, sieve and store solids at room temperature.

2.3. Characterization of Synthesized Cero- and Titanium Cero- Antimonates:

Fourier Transform Infrared Spectra (FT-IR) for synthesized materials were measured using Bomem FTIR spectrometer model BOMEM, MB-Series. The measurement carried out by KBr disc method technique from 400 to 4000 cm^{-1}.

X-ray diffraction patterns (XRD) of the synthesized materials were recorded using Shimadzu XD-D1 spectrometer with Cu-K_α radiation tube (λ = 1.5418 Å) and 30 Kv, 30 mA. The patterns and the intensity with d-spacing value tables printed out for calculation of the crystallite size and strain of the samples. The crystal system for the structure was determined.

Thermogravimetric analysis (TGA) (loss of ignition LOI) carried out by heating different samples at different heating temperatures in muffle furnace for 4 h. The weight loss (loss of ignition) calculated by the following expression;

$$\%\ Weight\ loss\ (\%\ loss\ of\ ignition) = \frac{W_i - W_f}{W_i} \times 100$$

Where W_i and W_f are the initial and final weight after ignition.

An elemental analysis for the synthesized materials investigated by X-ray fluorescence technique, Philips X-ray Fluorescence PW-2400 Sequential Spectrometer. Samples were prepared for measurement process as reported earlier [13] by grained 1.0 gram of the solid sample to very fine particles and mixed with poly vinyl-metha-acrylate as a binder to facilitate the pressing process. The mixture pressed in pressing machine to 20 psi for 30 sec. The measurement carried out using Super Q-Quantitative analysis program.

2.4. Applications of Cero- and Titanium Cero-Antimonates for the Removal of Heavy Metals

Applications of cero- and titanium cero- antimonates for the removal of heavy metals (Cu^{2+}, Zn^{2+}, Ni^{2+} and Cd^{2+}) in terms of the capacity measurements were carried out by equilibration batch technique. The experiment was done by shaking 0.1 M chloride salt solutions of the desired cations with a definite weight of the solid (batch factor V/m = 100 ml/g) for 3 h (time required to attain equilibrium). After equilibrium, solids separated and the concentrations of the cations were determined. The capacity calculated from the following relation;

$$\boldsymbol{Capacity} = (\%\ \boldsymbol{Uptake}/\boldsymbol{100}) \cdot \boldsymbol{C_o} \cdot \boldsymbol{V}/\boldsymbol{m} \qquad \boldsymbol{mmol}/\boldsymbol{g}$$

Where

$$\%\ Uptake = \{(C_o - C_f)/C_o\}.100$$

C_o and C_f are the initial and final concentrations of the cations, respectively,

V is the solution volume and m is the mass of the solid.

3. Results and Discussion

3.1. Structural and Crystallographic Features

Infrared data of cero-antimonate and titanium cero-antimonate were represented in **Table 1**. The spectra data in **Table 1** indicated strong and broad bands in the region 3500-2600 cm^{-1} for cero-antimonate and titanium cero-antimonate ion exchangers that may related to interstitial water molecules and OH groups [14-17]. The peaks at 1640 cm^{-1} and 1640-1440 cm^{-1} for cero-antiomante and titanium cero-antimonate, respectively may be due to free water molecules (water of crystallization) and being representative of strongly -OH groups in the matrix. Both cero-antimonate and titanium cero-antimonate ion exchangers show strong peaks at 1420 and ~1150 cm^{-1} that indicates the presence of Sb-OH and δ-Sb-OH groups [14-17]. Doping in situ precipitation of titanium ions

Table 1. IR spectra data of cero- antimonate and titanium cero- antimonate ion exchanger.

Experimental transmittance bands, cm^{-1}		Groups
Cero- antimonate	Titanium cero- antimonate	
Broad band at 3200-2800	Strong broad band at 3500-2600	H_2O [14-17]
1640	Strong bands at 1640-1440	H_2O [14-17]
1420	1420	Sb-OH [14-17]
1325	1300-1330	Ce-O [14-17]
1150	1100-1250	δ-Sb-OH [14-17]
	700-820	Ti-O [14-17]
650-450	650-450	Metal-Metal [14-17]

with cero-antimonate caused a smaller shift for δ-Sb-OH group to 1100-1250 cm^{-1} in titanium cero-antimonate ion exchanger [14-17]. Also, the peak related to Ti-O bond was appeared in the spectra of titanium cero-antiomnate at 700-820 cm^{-1} [14-17]. In addition, the peaks at 450-650 cm^{-1} related to metal-metal (M-M) bonds were appeared in both spectra of cero-antimonate and titanium cero-antiomnate ion exchangers [14-17].

X-ray diffraction patterns of crystalline cero-antimonate and titanium cero-antimonate were shown in **Figures 1** and **2**. From XRD data in **Figures 1** and **2**, it is clear that cero-antimonate has a crystalline structure and the crystalinity increased by the deposition of Ti ion with cero-antimonate (**Figure 2**). In addition, **Figures 1** and **2** indicate pure single phase of crystalline cero-antimonate and titanium cero-antimonate. According to this data, there is a clear evidence for the distribution of Ti ions in cero-antimonate. This clearfield from the peaks related to titanium (2 1 0) and (2 2 1) that appeared in **Figure 2** besides the peaks corresponding to Sb (1 1 1), Ce (2 2 0) and (3 3 1). Analyses of X-ray diffraction patters in **Figures 1** and **2** with JCPSD indicated that both cero-antimonate and titanium cero-antimonate belongs to cubic phase system.

The patterns in **Figures 1** and **2** revealed a number of peaks corresponding to Ce, Sb and Ti. The pattern in **Figure 1** shows six main peaks increases to eight peaks by doping of titanium ions in situ cero-antimonate (**Figure 2**). The intensity of peaks for cero-antimonate and titanium cero-antimonate and the peak data of titanium cero-antimonate were represented in **Table 2** and **Figure 3**, respectively. From these data we found that doping in situ precipitation of titanium with cero-antiomnate leads to create a new two peaks at 2θ ~ 45.75 and 52.56. Analyses of the data obtained according to Joint Committee for Powder Standard Diffraction (JCPSD) cards indicated that these peaks are corresponding to Sb (1 1 1), Ce (2 2 0) and (3 3 1), Ti (2 1 0) and (2 2 1), respectively, with cubic phase. The peaks related to titanium (2 1 0) and (2 2 1) are appeared in **Figure 2** and leads to increasing the intensity of the peaks related to cero-antimonate.

The interlayer spacing (d) has a definite relation to its plane indices with a cubic system of these ion exchangers. Consequently, there is a definite relation between the lattice plane (h k l) of the crystal and the diffraction angle 2θ. In cero-antimonate and titanium cero-antimonate ion exchangers the crystals belongs to cubic system. According to Bragg's equation;

$$2\,d\,\sin\theta = nl$$

Where;

d is interlayer spacing between two layers.

θ is the diffraction angle.

λ is the X-ray wavelength used of Cu-Kα tube.

And in cubic system (n = 1), therefore

$$\frac{1}{d^2} = \frac{h^2 + k^2 + l^2}{a^2}$$

then the lattice constant (a_o) can be calculated from the following equations:

$$\sin^2\theta = \frac{2\left(h^2 + k^2 + l^2\right)}{4{a_o}^2}$$

Or,

$$a_o = \left\{d^2\left(h^2 + k^2 + l^2\right)\right\}^{0.5}$$

This equation indicates the direction of the X-rays diffracted by (h k l) plane in a cubic lattice whose lattice constant (a_o). That is to say, diffractions are determined solely by the shape and size of the unit cell. On the contrary, we can possibly determine the shape and size of its unit cell about an unknown crystal by measurements of the directions of diffracted beams. The size and shape of the unit lattice can be described using the Miller indices h, k and l as shown in **Table 2**. These Miller indices define the lattice and are called the crystallographic axes of the cell. By analysis the X-ray diffraction data for cero-antimonate and titanium cero-antimonate, lattice constant (a_o) was calculated and found to 5.15 Å and 5.149 Å for cero-antimonate and titanium cero-antimonate, respectively. The data obtained also showed that the lattice constant (a_o) for cero-antimonate (5.15 Å) is slightly higher than titanium cero-antimonate (5.149 Å).

Attempts made to determine the crystallite size and

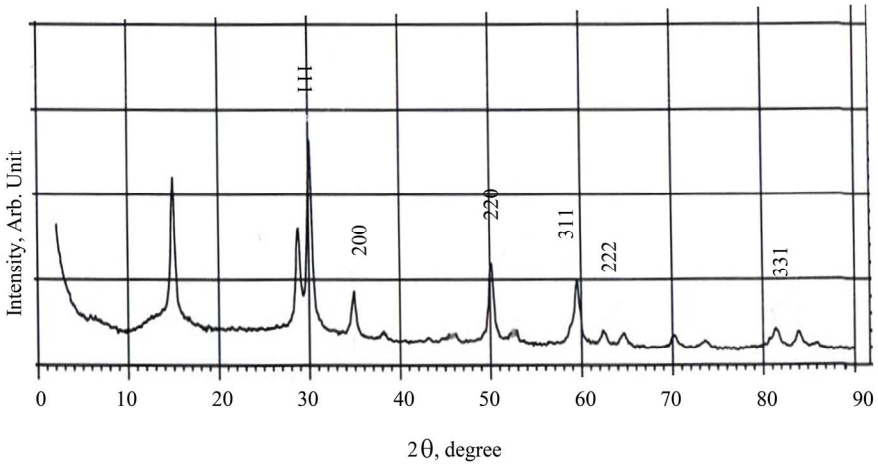

Figure 1. X-ray diffraction pattern of cero- antimonate ion exchanger at 25 ± 1°C.

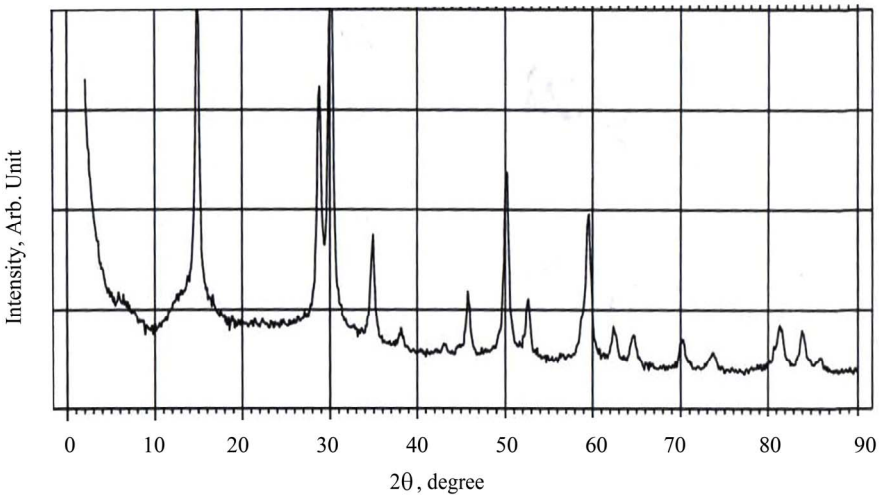

Figure 2. X-ray diffraction pattern of titanium cero- antimonate ion exchanger at 25 ± 1°C.

Table 2. X-ray data of cero- antimonate titanium cero- antimonate ion exchangers.

2θ (deg)	Cero- antimonite						Titanium cero- antimonate					
	D (Å)	I/Io	H	k	l	a_o (Å)	d (Å)	I/Io	h	k	l	a_o (Å)
30.04	2.972	100	1	1	1	5.148	2.972	100	1	1	1	5.148
34.83	2.573	23	2	0	0	5.146	2.573	23	2	0	0	5.146
45.75	--	--	--	--	--	--	1.981	17	2	1	0	5.147
52.56	--	--	--	--	--	--	1.739	17	2	2	1	5.147
50.07	1.820	55	2	2	0	5.148	1.820	55	2	2	0	5.148
59.46	1.553	44	3	1	1	5.151	1.553	44	3	1	1	5.151
62.33	1.488	11	2	2	2	5.155	1.488	11	2	2	2	5.155
81.31	1.182	13	3	3	1	5.152	1.182	13	3	3	1	5.152
Lattice constant (a_o)						5.15 Å	**Lattice constant (a_o)**					5.149 Å

strain from the XRD results using Hall equation [18].

$$b_{ps}Cos\theta = (\lambda/t) + K_{\varepsilon}Sin\theta$$

where, t is the crystallite size, λ is the X-ray wavelength used, β_{ps} is the angular line width of half-maximum intensity and θ is Bragg's diffraction angle and K_ε is the strain.

The crystallite size and strain effect on line broadening can be separated by plotting β_{ps} Cos θ versus Sin θ (as shown in **Figure 4**) in which slope K_ε is related to the strain and intercept (λ/t) is related to crystallite size. The experimentally determined crystallite size and strain were calculated and summarized in **Table 3**.

From data in **Table 3** we found that, the crystallite sizes of cero-antimonate and titanium cero-antimonate equal 0.792 and 0.841 nm, respectively, and the strain

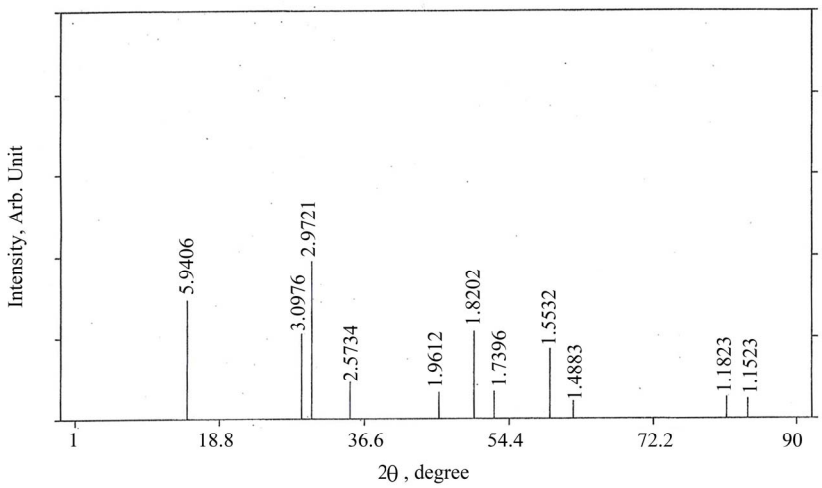

Figure 3. Peak data for X-ray diffraction pattern of titanium cero- antimonate ion exchanger at 25 ± 1°C.

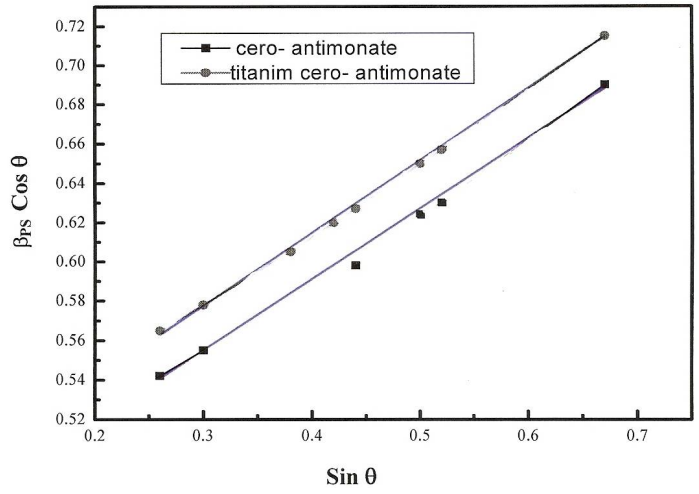

Figure 4. Plots of $\beta_{PS}Cos\theta$ against $Sin\theta$ for cero-antimonate and titanium cero- antimonite ion exchangers at 25 ± 1°C.

Table 3. Crystallite size and strain of cero-antimonate and titanium cero-antimonate ion exchangers at 25 ± 1°C.

Ion exchanger	Crystallite size (nm)	Strain
Cero-antimonate $CeSb_4O_{12}\cdot 6.19H_2O$	0.792	3.55
Titanium cero-antimonate $TiCeSb_4O_{14}\cdot 12.22H_2O$	0.841	3.22

equal 3.55 and 3.22 for cero-antimonate and titanium cero-antimonate, respectively. It can note that the strain in titanium cero-antimonate are higher these of cero-antimonate that may be related to doping in situ precipitation of titanium with cero-antimonate. Also **Table 3** indicated that the strain in ion exchangers increases as the crystallite size decreased which is an unusual phenomenon [19]. Owing to the large number of grain boundaries and the concomitant short distance between them, the intrinsic strains associated with such interfaces are always present in nano and crystalline structural materials.

Calcinations of both cero-antimonate and titanium cero-antimonate carried out by heating of 0.1 g of the solids at 850°C in muffle furn ace oven. The data obtained indicated that the overall loss of ignition from cero- antimonite is lower than that obtained for titanium cero-antimonate. This loss of ignition may attribute to loss of water and evaluation of some gases that accompanied to transformation of the solids. This behaviour can be interpretation as during the in situ precipitation of titanium with cero-antimonate, a large cavities can created in the matrix and traps a large amount of water that can pass to outside during the heating process.

The molar ratio of Ce:Sb in cero-antimonate and Ti:Ce:Sb in titanium cero-antimonate was estimated by X-ray fluorescence technique. The measurements were carried out using Semi-Q program as reported earlier [13]. The data obtained indicated that the percent ratio's of Ce to Sb in cero-antimonate equal 1.00 to 4.00, re-

spectively, while in titanium cero-antimonate the percent ratio's of Ti:Ce:Sb found to 1.00:1.00:4.00, respectively. From the data obtained from IR, XRD, XRF, TGA the tentative formula's for cero-antimonate and titanium cero-antimonate can predict as $CeSb_4O_{12}{\cdot}nH_2O$ and $TiCeSb_4O_{14}{\cdot}nH_2O$, respectively.

From the loss of ignition (X) of two solids at 150°C, the number of external water molecules (n) can calculate. As indicated from TG analyses, an X values for cero-antimonate and titanium cero-antimonate are equal 18.75% and 23.5%, respectively. The values of (n), the external water molecules, can be calculated using Alberti's equation [20];

$$18n = \frac{X\left(M + 18n\right)}{100}$$

where X is the percent weight loss in the ion exchanger at 150°C, and (M+18n) is the molecular weight of the material. The calculation gives the number of water molecules (n) per molecule of the solid and found to be 6.19 and 12.22 for cero-antimonate and titanium cero-antimonate, respectively. Then the tentative formula's for cero-antimonate and titanium cero-antimonate can rewrite as $CeSb_4O_{12}{\cdot}6.19H_2O$ and $TiCeSb_4O_{14}{\cdot}12.22H_2O$, respectively.

By using all data obtained and ChemDraw Ultra program software, we can predict construction the modeling of cero-antimonate and titanium cero-antimonate ion exchangers as shown in **Figures 5** and **6**.

The ion exchange capacities for Zn^{2+}, Cu^{2+}, Ni^{2+} and Cd^{2+} ions on cero-antimonate and titanium cero-anti-

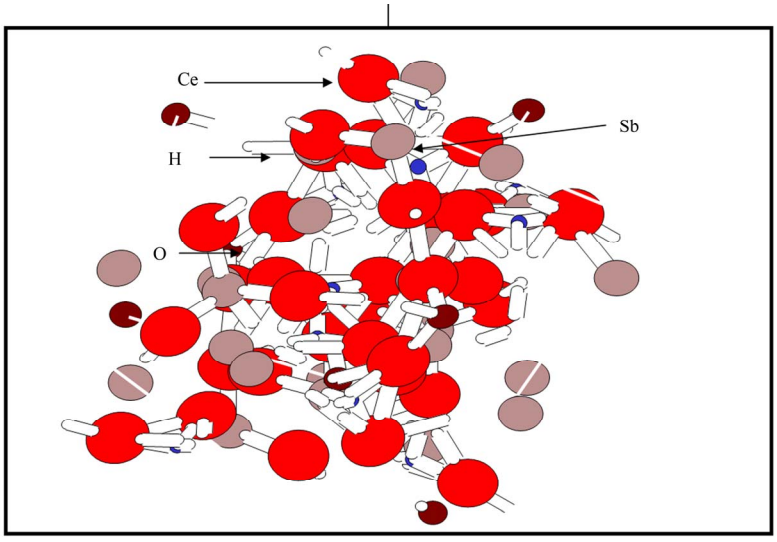

Figure 5. Structure of cero- antimonate.

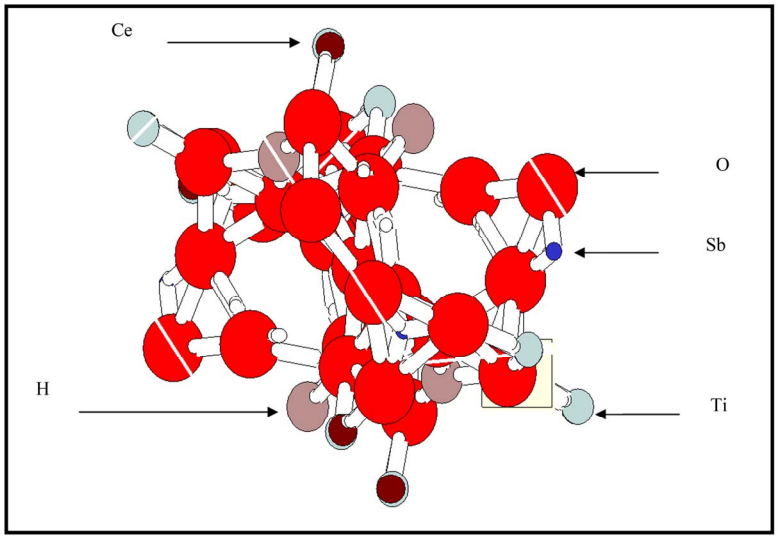

Figure 6. Structure of titanium cero- antimonite.

Table 4. Capacity of cero-antimonate and titanium cero-antimonate ion exchangers for some heavy metals at 25 ± 1°C.

Ion exchanger	Cation	Capacity, mmol/g
Cero-antimonate $CeSb_4O_{12}\cdot 6.19H_2O$	Cu^{2+}	0.25
	Zn^{2+}	0.46
	Cd^{2+}	0.55
	Ni^{2+}	1.00
Titanium cero-antimonate $TiCeSb_4O_{14}\cdot 12.22H_2O$	Cu^{2+}	0.41
	Zn^{2+}	0.62
	Cd^{2+}	0.82
	Ni^{2+}	1.11

monate were investigated and the data obtained was represented in **Table 4**. This table shows that the ion exchange capacity of cero-antimonate for heavy metals are increased by doping in situ precipitation of titanium ions with cero-antimonate with the same order of selectivity in both ion exchangers as, $Ni^{2+} > Cd^{2+} > Zn^{2+} > Cu^{2+}$. This selectivity order indicates that changes in the hydration of metal ion play a dominant ro;e in determining the selectivity of the exchange. This suggest that the energy required for the dehydration of the metal ions that can occupy a site in the ion exchanger plays an important role in the determining the selectivity series for the heavy metal ions [21]. On the other hand, according to the principle of hard and soft acids and bases (HSAB), hard acids prefer to bind to hard bases and soft acids to soft bases [21]. The hydrated cero-antimonate and titanium cero-antimonate can act as a Lewis base and the heavy metal ions as Lewis acids. The softness of the cations increases as the ionic radius of the heavy metal ions increases. The interaction of the heavy metal ions with the hydrated cero-antimonate and titanium cero-antimonate acting as a soft base, could be expected to increase with an increase in the ionic radii. **Table 4** also, shows a higher capacity values for the studied heavy metal ions on titanium cero-antimonate compared to cero-antimonate. This behaviour may attribute to the in situ precipitation of titanium with cero-antimonate leads to create large cavities that filled with a large amount of exchangeable water molecule. This amount of water a part of which are replaced with the exchanging cations and the other make flexibility for the flowing of exchanging cations inside the pores. From this study, we can conclude that, the in situ precipitation titanium with cero-antimonate leads to improvement of the structure of the solid and an increase in the capacity of cero-antimonate ion exchange.

4. References

[1] V. D. A. Cardso, A. G. D. Souza, P. C. Patricia and L. M. Nunes, "The Ionic Exchange Process of Co^{2+}, Ni^{2+} and Cu^{2+} in Alkaline and Acid Layered Titanates," *Colloids and Surfaces A: Physicochemical and Engineering Aspects*, Vol. 248, 2003, pp. 85-94.

[2] L. N. Nunes, A. G. de Souza and R. F. de Farias, "Synthesis of New Compounds Involving Layered Titanates and Niobates with Cu^{2+}," *Journal of Alloys and Compounds*, Vol. 319, 2001, pp. 94-99. doi:10.1016/S0925-8388(00)01414-6

[3] Y. H. Ni, A. W. Ge and Z. C. Zhang, "Preparation and Characterization of ZnS/Poly(Acrylamide-co-Acrylic Acid) Dendritical Nanocomposites by γ-Irradiation, *Materials Sciences and Engineering B*, Vol. 119, 2005, pp. 51-54. doi:10.1016/j.mseb.2005.01.003

[4] J. Lehto, K. Vaaramaa and H. Leinonen, "Ion Exchange of Zinc on an Aminophosphate Chelating Resin," *Reactive and Functional Polymers*, Vol. 33, 1997, pp. 13-18. doi:10.1016/S1381-5148(97)00002-3

[5] S. Y. Kang, J. U. Lee, S. H. Moon and K. Y. Kim, "Competitive Adsorption Characteristics of Co^{2+}, Ni^{2+} and Cr^{3+} by IRN-77 Cation Exchange Resin in Synthetized Waste Water," *Chemoshere*, Vol. 56, 2004, pp. 141-147. doi:10.1016/j.chemosphere.2004.02.004

[6] R. Koivula, J. Lehto, L. Pajo, T. Gale and H. Leinonen, "Purification of Metal Plating Rinse Waters with Chelating Ion Exchangers," *Hydrometallurgy*, Vol. 56, 2000, pp. 93-108. doi:10.1016/S0304-386X(00)00077-3

[7] I. M. El-Naggar and M. M. Abou-Mesalam, "Novel Inorganic Ion Exchange Materials Based on Silicates; Synthesis, Structure and Analytical Applications of Magneso-Silicate and Magnesium Alumino-Silicate Sorbents," *Journal of Hazardous Materials*, Vol. 149, 2007, pp. 686-692. doi:10.1016/j.jhazmat.2007.04.029

[8] I. M. El-Naggar and M. M. Abou-Mesalam, "Synthesis, Characterization and Ion Exchange Properties of Lithium Zirconium Silicate as Inorganic Ion Exchanger," *Arab Journal of Nuclear Sciences and Applications*, Vol. 38, No. 3, 2005, pp. 49-60.

[9] M. M. Abou-Mesalam, "Sorption Kinetics of Cu^{2+}, Zn^{2+}, Cd^{2+} and Ni^{2+} Ions on Synthesized Silico-Antimonate Ion Exchanger," *Colloids and Surfaces A: Physicochemical and Engineering Aspects*, Vol. 225, 2003, pp. 85-94. doi: 10.1016/S0927-7757(03)00191-2

[10] M. M. Abou-Mesalam and I. M. El-Naggar, "Diffusion Mechanism of Cs^{+}, Zn^{2+} and Eu^{3+} Ions in the Particles of Zirconium Titanate Ion Exchanger Using Radioactive Tracers," *Colloids and Surfaces A: Physicochemical and Engineering Aspects*, Vol. 215, 2003, pp. 205-211. doi: 10.1016/S0927-7757(02)00443-0

[11] M. M. Abou-Mesalam, M. M. Mostafa, M. M. Abdel-Aziz and I. M. El-Naggar, "Chemical Studies on the Retention of Some Heavy Metals from Simulated Waste Water Using Polymeric Species Impregnated Inorganic Ion Exchanger," *Arab Journal of Nuclear Sciences and Applications*, Vol. 38, No. 3, 2005, pp. 53-62.

[12] I. M. El-Naggar, M. M. Abou-Mesalam, M. M. El-Shorbagy and S. A. Shady, "Thermal and Chemical Stabilities of Some Synthesized Inorganic Ion Exchange Materials," *Arab Journal of Nuclear Sciences and Applications*, Vol. 39, No. 3, 2006, pp. 25-34.

[13] M. M. Abou-Mesalam and I. M. El-Naggar, "Chemical Deposition of Zirconium Doped Tin Silicate Ion Exchanger and Their Characterization," *Journal of Radio-*

analytical and Nuclear Chemistry, Vol. 279, No. 1, 2009, pp. 333-340. doi:10.1007/s10967-007-7281-9

[14] G. Socrates, "Infrared Characteristic Group Frequencies," Wiley, NJ, 1980.

[15] K. Nakamoto, "Infrared and Raman Spectra of Inorganic and Coordination Compound," John Willey and Sons, New York, 1978.

[16] R. N. Nyquist and R. O. Kagel, "Infrared and Raman Spectra of Inorganic Compounds and Organic Salts," Academic Press, New York, 1997.

[17] C. N. R. Rao, "Chemical Applications of Infrared Spectroscopy," Academic Press, New York, 1963.

[18] B. D. Culity and S. R. Steck, "Elements of X-Ray Diffraction," 3rd Edition, Prentice-Hall, Englewood Cliffs, NJ, 2001.

[19] A. S. Edelestein and R. C. Camarata, "Nanomaterials Synthesis Properties and Application," Institute of Physics Publishing, 1998, pp. 214, 230, 235, 241.

[20] G. Alberti, E. Torocca and A. Conte, "Stoicheiometry of Ion Exchange Materials Containing Zirconium and Phosphate," *Journal of Inorganic and Nuclear Chemistry*, Vol. 28, No. 2, 1996, pp. 607-613. doi:10.1016/0022-1902(66)80343-3

[21] M. M. Abou-Mesalam, "Sorption Kinetics of Cupper, Zinc, Cadmium and Nickel Ions on Synthesized Silico-Antimonate Ion Exchanger," *Colloids and Surfaces*, Vol. 222, 2003, pp. 85-94.

